

# Contents

<b>1</b>	<b>Background</b>	<b>3</b>
1.1	Anatomy of the spinal cord . . . . .	3
1.2	Principles of MRI . . . . .	4
1.3	Principles of Diffusion MRI . . . . .	7
1.4	Analysis of Diffusion MRI . . . . .	11
1.5	Summary . . . . .	20



# Chapter 1

## Background

### 1.1 Anatomy of the spinal cord

The spinal cord (SC) is the part of the central nervous system (CNS) that connects the brain and peripheral nervous system. It controls the voluntary movement of limbs and trunk, receives sensory information from these regions and monitors and coordinates the internal organ function in thorax, abdomen and pelvis.

The SC is protected by the vertebral column and is located inside the vertebral canal. In cross-section, the cord can be divided in two regions: (i) the peripheral region containing neuronal white matter tracts. (ii) the grey, butterfly-shaped central region made up of nerve cell bodies. This gray matter is centered around the central canal, containing cerebro-spinal fluid (CSF).

#### White matter architecture of the spinal cord

The white matter of the SC consists mostly of longitudinally running axons and glial cells. White matter axons are organized hierarchically grouped in bundles, tracts and pathways. Bundles of neighboring white matter axons that share similar features are called fibre bundles. A tract is formed by fibre bundles with same origin, course, termination and function. Multiple tracts with the same function form a pathway.

#### Ascending tracts

Figure ?? illustrates the location of the major ascending pathways in the SC. These sensory tracts, arise either from cells of spinal ganglia in the white matter of the SC or from intrinsic neurons within the gray matter that receive primary sensory input. The dorsal column hold the largest ascending tracts and are associated with tactile, pressure, and kinesthetic sense connecting with sensory areas of the cerebral cortex. Fibres of the spinothalamic tracts ascend in the lateral ventral part of the cord and convey signals related to pain and thermal sense. The anterior spinothalamic tract arises more anteriorly in the SC; conveying impulses related to light touch. At brain level the two spinothalamic tracts tend to merge and cannot be distinguished as separate entities. Anterior

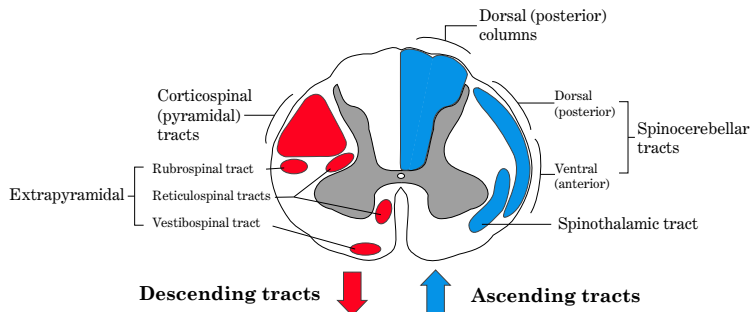


Figure 1.1: Illustration of the major ascending and descending fibre pathways of the SC (adapted from [http://en.wikipedia.org/wiki/Spinal\\_cord](http://en.wikipedia.org/wiki/Spinal_cord)).

and posterior spinocerebellar tracts are involved in automatic muscle tone regulation. These tracts ascend peripherally in the dorsal and ventral margins of the cord.

### Descending tracts

Tracts descending to the SC as illustrated in Figure 1.1 are concerned modulation of ascending sensory signals and are associated with voluntary motor function such as muscle tone and reflexes. The largest and most important, the corticospinal tract (CST), originates in broad regions of the cerebral cortex and descents in the lateral dorsal part SC white matter. Smaller descending tracts like the rubrospinal tract, the vestibulospinal tract, and the reticulospinal tract originate in small and diffuse regions of the midbrain, pons, and medulla and descend ventrally and laterally.

### White matter pathologies in the spinal cord

XXXX

## 1.2 Principles of MRI

Magnetic Resonance Imaging (MRI) is a non-invasive imaging method widely used in medicine. Since MRI is free of gamma-radiation (unlike CT or X-ray methods) it is one of the major tools for neuroimaging. MRI can describe tissue in terms of many different properties such as relaxation, density, and diffusion. Specifically, in this work we are interested mainly in the ability of MRI phenomena such as molecular motion and variation in the local magnetic fields. In this work we are mainly using the sensitivity of MRI to the molecular motion of water molecules experiments to infer information about the microscopic tissue morphology. A full account of MRI theory is beyond the scope of this work chapter and can be found elsewhere (?). However, a brief overview about the principles of MRI is given below.

## Magnetic resonance

The MR signal arises from the intrinsic magnetic moment and spin of certain nuclei. The hydrogen atom is most commonly used in MRI due to its abundance in the human body. When a hydrogen nucleus is placed in a magnetic field, its nuclear spin will begin to precess with a frequency governed by

$$\omega = \gamma \cdot B_0 \quad (1.1)$$

where  $\omega$  is the Larmor frequency,  $\gamma$  is the nucleus specific gyromagnetic ratio, and  $B_0$  is the magnetic field strength. When a radio-frequency (RF) pulse is applied perpendicular to the  $B_0$  field, with a frequency equal to the Larmor frequency (i.e. the resonance frequency) the magnetic proton spins tilt towards the transverse plane. Once the RF signal is removed, the nuclei realign themselves again parallel to the static  $B_0$  field. In MR terms the application of the RF pulse is called excitation and the following return to equilibrium is referred to as relaxation. The relaxation process is accompanied a loss of energy by the protons, which can be picked up by a receiving RF coil. This signal is referred to as the Free induction decay (FID) signal. Figure 1.2 illustrates this process. The FID, is characterized by two tissue specific time constants:

- T1 is the longitudinal relaxation time defined as the time it takes for the net magnetisation returns to the longitudinal equilibrium.
- T2 is the transverse relaxation time, i.e. the time that it takes for FID signal to decay due to randomly fluctuating internal magnetic fields caused by spin-spin interactions in the substance. This causes the spins to get out of phase and the transverse magnetization (and induced signal) is lost exponentially. In a non-idealized magnetic field, transverse magnetisation is also lost due to inhomogeneities in the  $B_0$  field, causing additional signal loss. The signal loss due to both spin-spin interference and  $B_0$  inhomogeneities is characterised by the time constant  $T2^*$ .

Usually the transverse magnetization decays more rapidly than it takes for the magnetisation to return to the longitudinal equilibrium. Both T1 and T2 are specific to the macromolecular environment of the protons and therefore are specific for different types of tissue, e.g. for different tissue types with the brain (GM T1/T2 = 950/100 ms, WM T1/T2 = 600/80 ms (17) and CSF XXXX). Furthermore, diseases such as cancer can alter the T1 and T2 of the tissue, and thus, T1 and T2 can be used to detect tissue affected by pathology.

## Spin-echo sequence

The simple spin echo (SE) sequence is the central pulse sequence of all experiments that are discussed in this dissertation. Figure 1.3 shows the layout of a simple SE experiment. The SE sequence starts with a 90° (P90) RF-pulse that flips magnetization in the transverse plane, followed by a 180° RF pulse (P180) after time TE/2 and the signal readout after another TE/2, producing an echo at time TE. The P180 inversion pulse will reverse the demagnetization by field inhomogeneities so that the contrast is mainly driven by spin-spin relaxation (T2). When TE is sufficiently small compared to the spin-lattice relaxation time T1 of the sample, normally taken care by long repetitions times ( $TR > 5 \times T1$ ), the obtained signal is called T2-weighted (T2w).

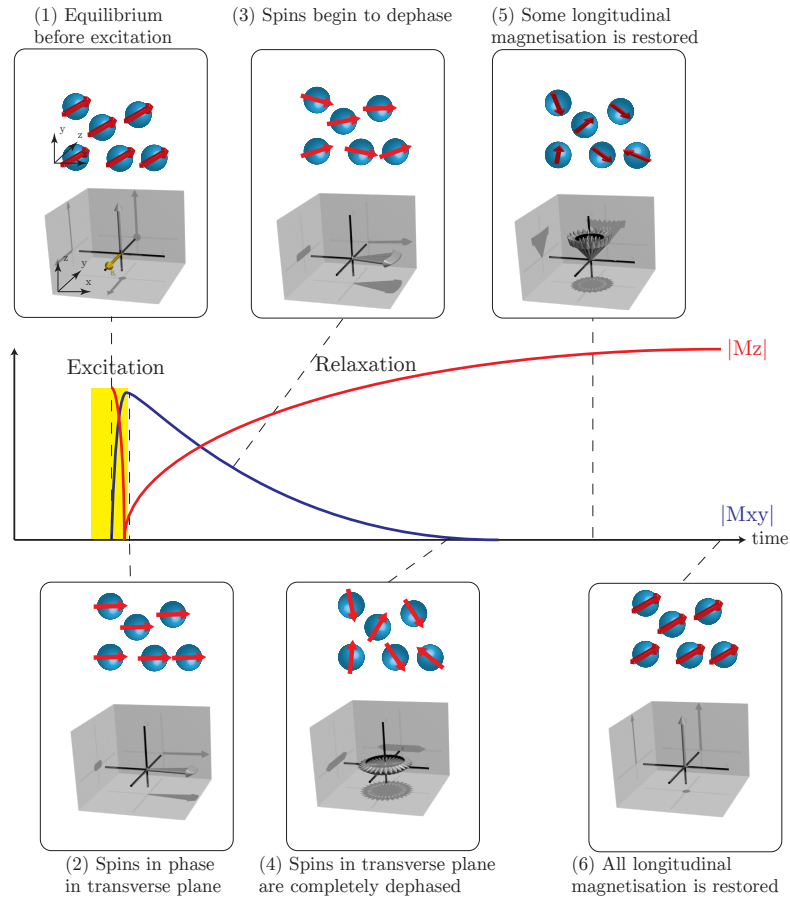


Figure 1.2: Simplified illustration of spins during different steps of the FID signal formation after a  $90^\circ$  RF pulse is applied. Some figures were created using the SpinBench software (?).

## Signal and Image formation

The MR signal is collected during relaxation, and it is the moving transverse magnetisation  $\mathbf{M}_{xy}$ , generated while the spins return to their original states. The MR signal we detect is called the Free Induction Decay or FID signal and is a signal which decays according to the  $T_2$  relaxation. The signal is

$$S(t) = \mathbf{M}_0 \exp\left(\frac{-t}{T_2}\right) \quad (1.2)$$

where  $\mathbf{M}_0$  is the steady-state magnetisation before any  $T_2$  decay.

To generate an image we first choose a slice by exciting a selection of spins, usually in the  $z$  direction. Within the slice we encode spatial information. To achieve that we need a gradient field  $\mathbf{G} = (G_x, G_y, G_z)$ . A gradient magnetic field is a small spatially varying magnetic field superimposed on  $\mathbf{B}_0$ . The gradient  $G_z$  causes protons at different locations along the gradient direction to precess at different frequencies, and only protons precessing with frequencies

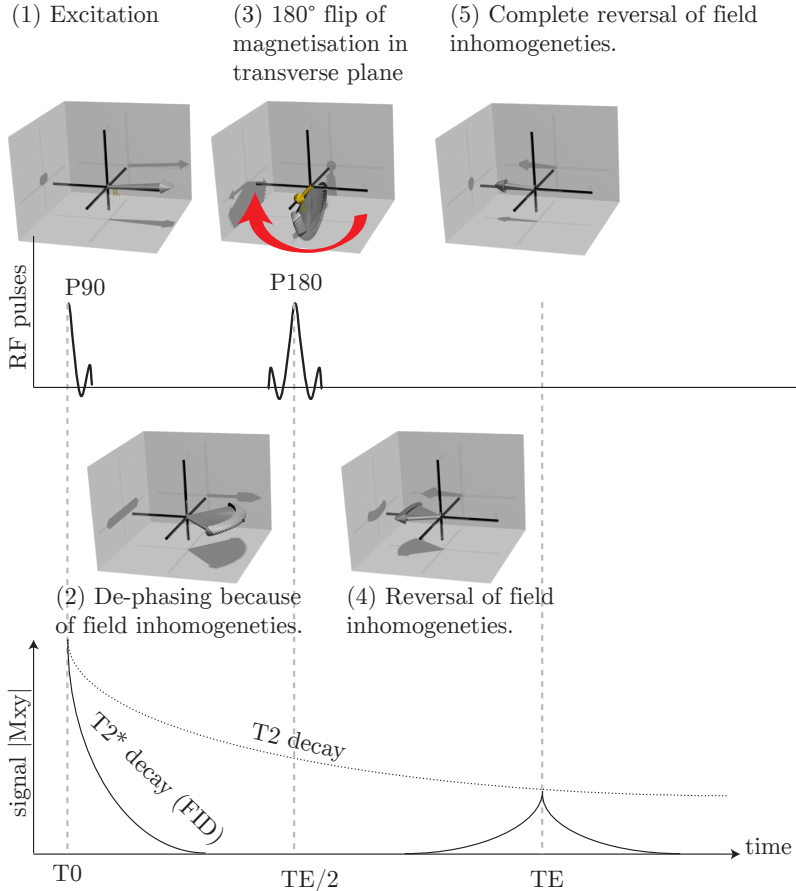


Figure 1.3: Simplified illustration of spins during different steps of the FID signal formation after a  $90^\circ$  RF pulse is applied. Some figures were created using the SpinBench software (?).

belonging to the range of the RF pulse sequence will be excited

$$\omega_0 = \gamma(\mathbf{B}_0 + \mathbf{G}(t)\mathbf{R}(t)) \quad (1.3)$$

where  $\mathbf{R}$  is the position of the spin at time  $t$ . The gradients  $G_x$  and  $G_y$  allows for spatial encoding within the slice. Thus, each  $x, y$ , pixel possesses a unique frequency which encode the spatial location of the pixel in the image. The signal is then received in frequency space, or k-space. The frequency information is then reconstructed into an image using a Fourier Transform ?.

### 1.3 Principles of Diffusion MRI

Diffusion MRI is a relatively recent field of research with a history of more or less twenty years. Diffusion MRI is of growing interest because it helps understand functional coupling between cortical regions of the brain, which is

useful in characterization of neuro-degenerative diseases, in surgical planning and in other medical applications. The great success of diffusion MRI comes from its capability to describe the geometry of the underlying microstructure. To do so, diffusion MRI captures the average diffusion of water molecules, which probes the structure of the biological tissue at scales much smaller than the imaging resolution. The diffusion of water molecules is Brownian under normal unhindered conditions, but in fibrous structure such as white matter, water molecules tend to diffuse along fibers. Due to this physical phenomenon, diffusion MRI is able to obtain information about the neural architecture *in vivo*. It is also the only imaging modality so non-invasively. We now review the basics physical principles of diffusion MRI.

### 1.3.1 Brownian motion

At a microscopic scale, water molecules freely move and collide with each other in an isotropic medium according to Brownian motion [Brown (1828)]. At a macroscopic scale, this phenomenon yields a diffusion process. In a typical diffusion MRI experiment the spatial dimension of the prescribed voxel is several magnitudes bigger than the length scale of diffusion motion. Hence it is useful to consider the average displacement probability density function (dPDF) (often referred to as the “average propagator” (Kärger and Heink, 1983)), describing the ensemble average probability of a particle moving the distance during diffusion time independent of starting position within a sample. In the simplest case of pure molecules motion in the absence of any impeding barriers, the diffusion process can be simply be characterised by the diffusion coefficient  $D(?)$ . In an isotropic medium, the diffusion coefficient  $D$  was related by Einstein [Einstein (1956)] to the root mean square of the diffusion distance as

$$EINSTEIN \quad (1.4)$$

where  $\tau$  is the diffusion time,  $\langle \dots \rangle$  denotes the ensemble average and  $R = r - r_0$  is the net displacement vector between the original position  $r_0$  of a particle and the position  $r$  after the time  $\tau$ .

### 1.3.2 Free, hindered and restricted diffusion in biological tissue

Diffusion in nervous tissue can deviate significantly from simple Gaussian behavior in the presence of cell membranes and structures that hinder or restrict diffusion of water molecules (Bihan, 1995).

In the simplest case, free diffusion (or unrestricted diffusion) describes the pure Brownian motion of water, i.e. molecules diffusing freely in all directions without in the absence of any boundaries. In reality, free diffusion is rarely encountered in a biological tissue sample. Instead, the presence of restricting barriers, such as cell walls, membranes or axonal myelin sheaths impede the motion of the water molecules and alters their displacement pattern. In this case, the diffusion pattern is not only influenced by the diffusivity of the medium but more importantly informs about the characteristics of the surrounding environment on the scale of the mean displacement.

The observed effects on the diffusion MR signal can be quite diverse, depending on type and location of barriers within the sample. It is helpful to

further distinguish between restricted and hindered diffusion (see Figure 1 for illustration). Restricted diffusion is observed if the movement of water molecules is confined in closed spaces, such as impermeable cells wall. Those molecules experience restricted diffusion in that the molecules cannot displace farther than the confines of the cell. In hindered diffusion, the water movement of molecules is impeded however not confined within a limited space. Hindered diffusion best describes water motion in the space between densely packed cells or axons.

### The Stejskal-Tanner PGSE experiment

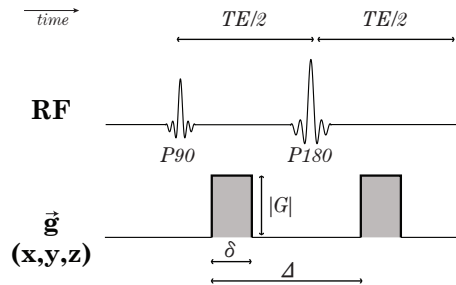


Figure 1.4: Pulse sequence diagram of PGSE sequence. Imaging and acquisition gradients are omitted for clarity.

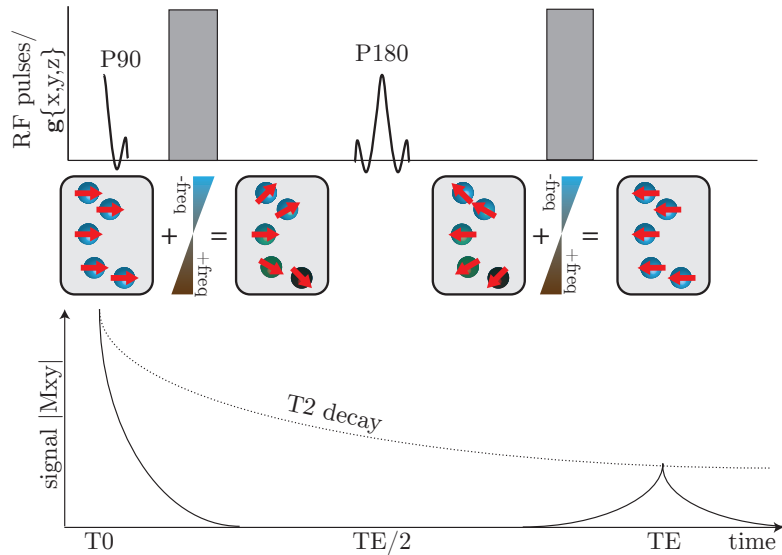
By using a certain pulse sequence the MRI signal can be made sensitive to the molecular motion of the water molecules within the tissue, providing contrast about the molecular motion on a voxel scale. The most commonly used pulse sequence is pulsed gradient spin echo (PGSE) sequence, introduced by (?). The PGSE is based on the standard SE sequence described above with an additional pair of identical diffusion weighting gradients, which make the sequence sensitive to the diffusion of water molecules (see Figure 1.4). Figure 1.5 illustrates the principle of diffusion encoding using the PGSE sequence. The first diffusion gradient adds a phase offset dependent on each molecule's position. If the molecule's position doesn't change, the second diffusion gradient will reverse the phase offset (see Figure 1.5a). However, in the case of motion due to diffusion, the individual positions will differ between the first and second diffusion gradient, resulting in a reduced signal amplitude (see Figure 1.5b). The degree of signal loss is dependent on the rate of diffusion in the tissue but is also controlled by the parameters of the PGSE sequence, namely:

- the diffusion gradient strength ( $|G|$ ) and diffusion gradient direction ( $\vec{g}$ ),
- the diffusion gradient pulse duration ( $\delta$ ),
- the diffusion time ( $\Delta$ ) between both gradient pulses.

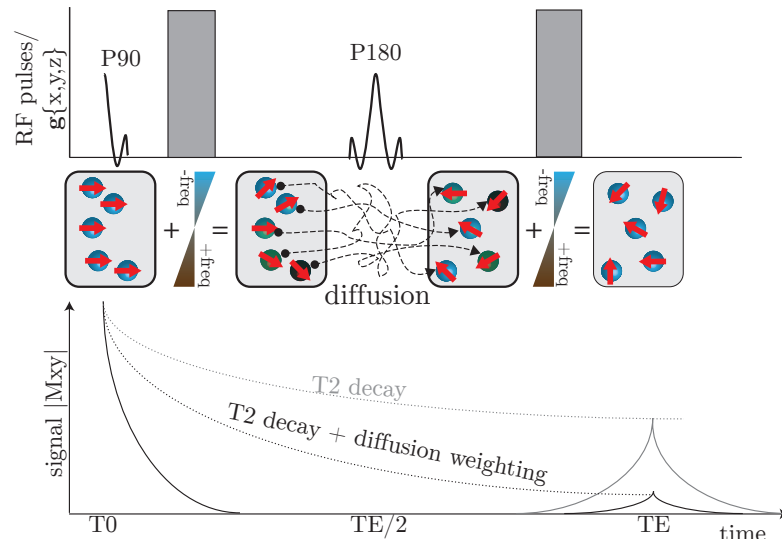
In the literature the combination of those PGSE parameters is often summarised in terms of the diffusion weighting factor  $b$ -value, which is defined as:

$$b = \gamma^2 |G|^2 \delta^2 (\Delta - \frac{\delta}{3}), \quad (1.5)$$

where  $\gamma$  is the gyromagnetic ratio.



(a) Spin phase distribution in case of no molecule motion. The phase dispersion introduced by the first diffusion gradient is completely reversed by the second diffusion gradient.



(b) Spin phase distribution in case of diffusing molecules during the diffusion time  $\Delta$ . Because of motion, the individual molecules experience different phase offsets at the first and second diffusion gradients. As a result, there remains some phase incoherence after the second diffusion gradient, which culminates into an attenuation of the total spin echo response.

Figure 1.5: Cartoon of the principle of diffusion encoding in the PGSE experiment. The diagrams present the spin development over the course of the sequence in the case of: (a) no diffusion or (b) diffusing molecules.

## 1.4 Analysis of Diffusion MRI

Cleveland (?) was the first to detect anisotropic diffusion in excised skeletal muscle, with diffusion MR. It was not until 1990 however that images of diffusion anisotropy were obtained *in vivo* by Moseley in the cat spinal cord (37) and Doran and Chenevert in cerebral white matter (38, 39). The introduction of the diffusion tensor model gave rise to the systematic analysis of the diffusion MRI signal. In the following we will discuss some of the most common diffusion MRI methods, with particular focus on those techniques that were used in this dissertation.

Most commonly, diffusion MRI is processed in terms of a model-based analysis, i.e. using a mathematical description of the diffusion signal that can be referred back to the tissue properties. It makes sense to describe any such model-based analysis pipeline with regard to its main building blocks:

**Acquisition:** The set of actual diffusion MR measurements. Any quantitative analysis of the diffusion MRI signal usually needs of many samples of different PGSE parameters, e.g. many different gradient encoding directions and/or  $|G|, \delta, \Delta$  combinations. We formally define such a combined set of  $n$  singular PGSE acquisitions as a protocol ( $\mathcal{P}$ ):

$$\mathcal{P} = \{(\vec{g}_1, |G|_1, \delta_1, \Delta_1), \dots, (\vec{g}_n, |G|_n, \delta_n, \Delta_n)\}, \quad (1.6)$$

or alternatively using the shortcut term  $b$  as:

$$\mathcal{P} = \{(\vec{g}_1, b_1), \dots, (\vec{g}_n, b_n)\}.$$

Several other terms are often found to describe selected properties of a acquisition protocol. A gradient scheme usually describes a set of diffusion gradient directions only without specifying PGSE pulse parameters or  $b$ -values. The term High-angular-diffusion-imaging (HARDI) describes a special case of gradient scheme with a high number diffusion directions ( $>60$ ), which are uniformly sampled over the unit sphere (e.g. like Cook, Jones). A *shell* in the context of diffusion MRI refers to a protocol or subset of a protocol with several different gradient directions acquired at the same  $b$ -value.

Different analysis methods have different requirements on the acquisition protocol. While it suffices for some methods to acquire few samples of the PGSE parameter space, other methods require one or more HARDI shells with different  $b$ -values and/or many different  $(\vec{g}, |G|, \delta, \Delta)$  combinations.

**Diffusion model:** The diffusion model is a mathematical approximation of the diffusion process. The diffusion model usually is controlled by a set of feature parameters  $p$ , which can be (directly or indirectly) related back to the sample environment of the diffusion process. The diffusion model is usually associated closely with a mathematical formulation of the predicted diffusion MR signal for a given acquisition and set of diffusion model parameters.

**Fitting:** The fitting procedure links the observed signals from the acquisition to the diffusion model, with the aim to infer about the tissue properties of the scanner sample. In most case, a forward-modelling approach is applied, i.e., the acquired signal is fitted to a model that has been determined a-priori to find the particular set of model parameters that explains the acquired data best.

In the following section we will explain a selection of different models, with particular focus on the techniques used in this dissertation.

### 1.4.1 Short gradient approximation and the q-space formalism

If we assume the diffusion gradient pulse  $\delta$  sufficiently short, multiple times smaller than the diffusion time  $\Delta$ , any motion of water molecules during the diffusion encoding gradient time can be neglected. In the SGP regime, the diffusion echo attenuation  $S(|G|, \delta, \Delta)$  for a specific PGSE acquisition with parameters  $|G|, \delta, \Delta$  can be expressed as the integral of the net phase shifts over all water over all molecule positions ( $r$ ) weighted by the conditional probability  $P(r|r')$  of the molecules movement from position  $r$  to  $r'$ (?):

$$S(|G|, \delta, \Delta) = \int \int P(r)P(r|r', \Delta) \exp[-i \cdot \gamma \delta |G| \cdot (r' - r)] dr' dr, \quad (1.7)$$

with  $\gamma$  the gyromagnetic ratio of protons. We can now describe ensemble molecule motion pattern over one voxel by the average diffusion probability density function (dPDF) (often referred to as the average propagator(?)) as the ensemble average probability of a particle moving the distance  $R$  independent of its starting position:

$$\bar{P}(R, t) = \int P(r)P(r|R, t) dr. \quad (1.8)$$

We can now use the dPDF definition to express the diffusion signal attenuation by substituting Equation 1.8 in the Equation 1.7 as such:

$$S(|G|, \delta, \Delta) = \int \bar{P}(R, t) \exp[-i \cdot \gamma \delta |G| \cdot R] dR, \quad (1.9)$$

If we introduce the **q**-value (or wavenumber) as

$$\mathbf{q} = \frac{\gamma \mathbf{G} \delta}{2\pi}. \quad (1.10)$$

the signal equation can be written as:

$$S(q, \Delta) = \int \bar{P}(R, t) \exp[2\pi i \cdot q \cdot R] dR. \quad (1.11)$$

It is easy to see that the Equation 1.11 presents a simple Fourier relationship between the signal  $S$  and the dPDF. This relationship can be exploited in q-space analysis, where the diffusion signal is measured with many different q-values at a certain fixed diffusion time. The inverse Fourier transformation of the measured signal will then directly give the dPDF without the need to impose any constraints on its characteristics.

### 1.4.2 Q-space imaging

The combination of q-space analysis with MR imaging methods is called q-space imaging *q*-space imaging (QSI) (Callaghan, 1991; Assaf et al., 2000). QSI provides the full displacement probability profile in each voxel of the imaged volume. However, the visualization and quantification of the full displacement profile in each voxel is usually impracticable. Instead, it is more common to derive parameters from the dPDF that summarise the features of the displacement profile. The most widely used parameters are: zero displacement probability ( $P_0$ ), full width of half maximum (FWHM) and the kurtosis (K). Figure ?? illustrates the QSI analysis steps and resulting  $P_0$ , FWHM and K parameter maps.

The  $P_0$  and FWHM parameter describe the height and width of the displacement profile. Generally, high  $P_0$  and low FWHM can be interpreted as indicators of restricted diffusion; low  $P_0$  and wide FWHM are related to more free or hindered diffusion. The FWHM is of particular theoretical interest as it can be directly related to the size of the restricted compartment in simple geometries via the autocorrelation function (Cory, 1990; Kuchel et al., 1997). Some studies report the root mean square displacement (RMS) instead of FWHM. (Cory and Garroway, 1990) suggest the conversion between FWHM and RMS as  $RMS = 1.443 \cdot FWHM$ . However, the equality is only true if the diffusion profile is truly Gaussian.

The kurtosis parameter (here defined as the excess kurtosis (Kenney and Keeping, 1957)) describe how much a distribution differs from the normal distribution. Kurtosis is defined as the standardised fourth central moment of a distribution minus 3 (to make the kurtosis of the normal distribution equal to zero). For a finite sample of n datapoints the kurtosis K is computed as:

$$K = \frac{1}{n} \sum_{i=1}^n [(x_i - \bar{x})^4] / [(1/n) \sum_{i=1}^n (x_i - \bar{x})^2]^2 - 3 \quad (1.12)$$

with  $\bar{x}$  being the sample mean. A high kurtosis distribution has a narrower peak and long, fat tail compared to a normal distribution. A low kurtosis distribution has a more rounded peak and a shorter, thinner tail. In the context of diffusion analysis, the kurtosis parameter can be used to quantify how much the dPDF differs from a Gaussian displacement distribution (Jensen and Helpern, 2010). High K values can therefore be interpreted as an indicator of restricted diffusion in a sample.

#### Limitations of QSI

QSI parameters measured in nervous tissue are often interpreted as a direct indicator of axonal architecture, such as the mean axon diameter (MAD). Early studies have demonstrated that q-space analysis can indeed provide exact estimates of the geometry in simple samples, e.g. yeast cells (Cory and Garroway, 1990) or blood cells (Kuchel et al., 1997). However, experiments on real nervous tissue have shown that the interpretation of q-space parameters in axonal tissue is more complicated (King et al., 1994; Assaf and Cohen, 2000; Assaf et al., 2000; Bar-Shir and Cohen, 2008). (Assaf and Cohen, 2000) were first to demonstrate that the displacement profile of nervous can be expressed as a combination of at least two compartments exhibiting hindered and restricted diffusion. A recent

study of QSI in the in-vivo human brain by (Nilsson et al., 2009) confirmed that the FWHM perpendicular to white matter fibres did not change with diffusion time. Parallel FWHM increased linearly with the square root of diffusion time, restricted and hindered diffusion, respectively, as expected from theory (Figure REF). The two compartments are often attributed to intra-cellular (IC) and extra-cellular (EC) water, although there is an ongoing debate over the interpretation of these results (see e.g. (Kiselev and Il'yasov, 2007; Mulkern et al., 2009)).

Since q-space analysis provides the average displacement probability over the whole voxel, the q-space measurement is affected by both IC and EC compartments as well as by the amount of exchange between the two. As a result, the displacement PDF may be broader than the actual MAD would suggest, due to the addition of displacements from hindered diffusion in the EC compartments. Other factors such as the distribution of sizes and variety of shapes further complicate the interpretation of q-space parameters to infer the real axon diameter distributions.

### 1.4.3 Apparent diffusion coefficient

In the absence of any diffusion impeding barriers, the dPDF takes the form of a simple Gaussian probability distribution, which is only dependent on the diffusion time  $t$  and the diffusion coefficient  $D$ :

$$P(\mathbf{r}_0, \mathbf{r}, \Delta) = \frac{1}{\sqrt{(4\pi dt)^3}} \exp\left(-\frac{|\mathbf{r} - \mathbf{r}_0|^2}{4dt}\right). \quad (1.13)$$

In true free diffusion, the  $D$  is simply the diffusion coefficient of the medium and the dPDF description is exact. However, in real biological tissue, virtually all molecules will have interacted with their environment within the timescale of a typical diffusion MR experiment. In this case the above expression is a just simple approximation of the underlying true dPDF and  $D$  above is not only related to the diffusivity of the medium but also informs about the diffusion impedance. To highlight the difference to the classical definition of the diffusion coefficient, we refer to  $D$  as the apparent diffusion coefficient (ADC).

The ADC model is based on the assumption that even in the presence of hindered or restricted diffusion, the dPDF remains Gaussian in nature. Therefore, the closed form solution for the dPDF can be substituted in the general q-space formalism given in Equation ??, simplifying it to:

$$\text{ADC formula}. \quad (1.14)$$

For convenience, in the literature the ADC model is often rewritten in terms of the  $b$ -value:

$$S(b) = S_0 \exp(-b \cdot \text{ADC}) \quad (1.15)$$

The parameters  $S_0$  and ADC are tissue dependent and can be estimated by acquiring a minimum of two diffusion weighted images with different  $b$ -values (usually  $b = 0$  and  $b = 800 - 1200 \text{ mm}/\text{s}^2$  for in-vivo nervous tissue). Using a simple log-transformation, Equation can rewritten as a linear equation:

$$\log(S(b)) = \log(S_0) - (b \cdot \text{ADC}), \quad (1.16)$$

which can be easily solved, e.g, using a linear least squares approach.

#### 1.4.4 Diffusion Tensor

In ordered tissue like white matter the diffusion will be directed, i.e., the ADC will depend on the direction  $\vec{g}$  of the applied gradient. The Equation 1.16 can be extended to reflect the in 3D by using the Diffusion Tensor (DT) formulation:

$$S(b, \vec{G}) = S_0 \exp(-b\vec{g}^T \mathbf{D}\vec{g}) \text{ with } \mathbf{D} = \begin{bmatrix} d_{xx} & d_{xy} & d_{xz} \\ d_{xy} & d_{yy} & d_{yz} \\ d_{xz} & d_{yz} & d_{zz} \end{bmatrix}. \quad (1.17)$$

Since the DT is positive symmetric, it requires one non-diffusion weighted measurement and a minimum of 6 different diffusion weighted measurements with non-coplanar gradient directions to fit the 7 free parameters of the model. However, we usually acquire more signals to overdetermine the solution, add noise control and increase directional resolution (?).

By an Eigen decomposition of the DT we obtain the three eigenvectors  $\vec{v}_1, \vec{v}_2, \vec{v}_3$  and their corresponding eigenvalues  $\lambda_1 \geq \lambda_2 \geq \lambda_3$ . The first eigenvector can be interpreted as the principal diffusion directions with  $\lambda_1$  being the principal diffusivity. Usually  $\lambda_1$  is also referred to as the axial diffusivity (AD) as it corresponds with the diffusivity parallel to white matter axons(?). Other commonly used DTmetrics are:

- The mean diffusivity (MD), computed as:

$$MD = \frac{\text{Tr}(D)}{3} = \frac{\lambda_1 + \lambda_2 + \lambda_3}{3}. \quad (1.18)$$

- The fractional anisotropy (FA) that represents the degree of diffusion anisotropy in each voxel. FA increases with directional dependence of particle displacements and is greatest when diffusion is highly directed. FA is computed by

$$FA = \sqrt{\frac{3}{2}} \frac{\sqrt{(\lambda_1 - MD)^2 + (\lambda_2 - MD)^2 + (\lambda_3 - MD)^2}}{\sqrt{\lambda_1^2 + \lambda_2^2 + \lambda_3^2}} \quad (1.19)$$

- The radial diffusivity (RD) is the average diffusivity perpendicular to the major diffusion direction:

$$RD = \frac{\lambda_2 + \lambda_3}{2}. \quad (1.20)$$

#### 1.4.5 Limitations of the SGP approximation

Unlike modern NMR spectrometers and pre-clinical small bore scanners, most clinical MRI systems are only equipped with limited maximal gradient strength (usually 40-60 mT/m). On these systems the necessary high q-values, e.g., needed for q-space analysis cannot be achieved without prolonged diffusion gradient pulse durations. (Mitra and Halperin, 1995) showed that the effective molecule displacement measured with a finite diffusion pulse is equivalent to the distance between the centre of mass (COM) of the molecule trajectories occurring while the diffusion gradients are applied. If the SGP condition «  $\Delta$  is fulfilled, the observed distance between the COMs of the trajectories is

approximately the same as the true displacement of the molecule. However, if  $\delta$  is long, molecules movement will occur during the diffusion gradient pulses and only the displacement between the COMs will be observed. As illustrated in Figure 3, in the case of restricted diffusion, this increase in gradient pulse duration will cause the underestimation of the true displacement. When implementing QSI protocols on a clinical scanner, one has to be wary of the effect of the finite gradient pulse duration and its implications. Usually, clinical studies of QSI have to violate the SGP condition to achieve sufficiently high q-values. As expected from the COM effect, this causes an artifactual reduction of the RMD. This has been confirmed in simulation (Linse and Soderman, 1995; Lätt et al., 2007b) and various experimental studies in phantoms (Avram et al., 2004; Lätt et al., 2007a), excised tissue (Malmborg et al., 2006; Bar-Shir et al., 2008) and even in in-vivo human scans (Nilsson et al., 2009). As a consequence, the estimated displacement profile has to be interpreted with caution as it will not reflect the true displacement in the tissue. The SGP violation is a fundamental problem in the above models and can only be avoided with an increase of the maximum gradient strength. As an additional advantage of stronger gradients, EPI read-outs can be shortened thereby decreasing the echo time and yielding gains in SNR and reducing susceptibility distortions.

Some experimental clinical scanners are already equipped with gradients systems capable of generating up to 300mT/m (Toga et al., 2012). However, those dedicated system are designed for a specific research project and the general availability of those strong whole body gradients in the future is doubtful due to their high costs. Economic feasibility aside, the use of higher gradient strengths and shorter pulse width also increases the risk of peripheral nerve stimulation (PNS) (REF) and might cause more discomfort for the subjects.

#### 1.4.6 Gaussian phase approximation

As discussed above, the SGP approximation is often impossible to fulfill on typical clinical scanners. An alternative model of the diffusion process is given by the Gaussian phase distribution (GPD). In contrast to the SGP, the GPD offers a description of the diffusion MR signal in the presence of finite  $\delta$  under the assumption that the phases of the spins due to the magnetic field gradients are Gaussian distributed.

In the SGP approximation we use the probability density function of spin displacements, whereas the GPD approximation considers the distribution function of spin phases  $P(\phi, \Delta)$  at the echo time TE having phase  $\phi$ . The total signal in terms of  $P(\phi, \Delta)$  is

$$S(\delta, \Delta, \mathbf{G}) = \int_{-\infty}^{+\infty} P(\phi, \Delta) \cos \phi d\phi. \quad (1.21)$$

For molecules undergoing free diffusion, characterised by a single diffusion coefficient  $D$ ,  $P$  is Gaussian so that the signal is

$$S(\delta, \Delta, \mathbf{G}) = \exp \left( -\gamma^2 |\mathbf{G}|^2 \delta^2 (\Delta - \delta/3) d \right), \quad (1.22)$$

### 1.4.7 Models of restriction

Murday and Cotts ? use the GPD approximation to derive an expression for the signal for particles diffusing in a spherical boundary of radius  $R$  specifically for the PGSE experiment with finite  $\delta$ . The signal is

$$\ln S = -2\gamma^2 \mathbf{G}^2 \sum_{m=1}^{\infty} \frac{2da_n^2\delta - 2 + 2e^{-da_n^2\delta} + 2e^{-da_n^2\Delta} - e^{-da_n^2(\Delta-\delta)} - e^{-da_n^2(\Delta+\delta)}}{d^2a_n^6(R^2a_n^2 - 2)} \quad (1.23)$$

where  $d$  is the free diffusion constant and  $a_n$  is the  $n$ th root of the Bessel equation  $(a_n R) J'_{3/2}(a_n R) - 1/2 J_{3/2}(a_n R) = 0$ , where  $J$  is the Bessel function of the first kind.

Stepisnik ? uses the same technique to derive analytic solutions for the signal in cylinders and in between planes with finite gradient pulses. The equation for the signal from particles diffusing within the cylinder of radius  $R$  is

$$\ln S = -2\gamma^2 \mathbf{G}^2 \sum_{m=1}^{\infty} \frac{2da_m^2\delta - 2 + 2e^{-da_m^2\delta} + 2e^{-da_m^2\Delta} - e^{-da_m^2(\Delta-\delta)} - e^{-da_m^2(\Delta+\delta)}}{d^2a_m^6(R^2a_m^2 - 1)} \quad (1.24)$$

where  $a_m$  is the  $m$ th root of equation  $J'_1(a_m R) = 0$  and  $J'_1$  is the derivative of the Bessel function of the first kind, order one. We note that this expression is often attributed to Van Gelderen ?.

### 1.4.8 Compartment models

In addition to the simple Gaussian diffusion model, discussed in section ??, various analytic solutions were developed for the diffusion signal in simple geometries such spheres, parallel planes (???) or cylinders (?). Using a-priori information about the microstructure of the investigated sample, the diffusion signal can be approximated by a combination of these simple geometric compartments. Each of the  $n$  different compartments possesses the model parameters  $\phi_i$  from which the signal  $S_i$  is computed. Each compartment is assigned a volume fraction  $f_i$  with  $0 \leq f_i \leq 1$  for all  $1 \leq i \leq n$ . The total signal for the model under the combined model parameter set  $\phi = \phi_1 \cup \dots \cup \phi_n$  is then given by:

$$S(\phi) = \sum_{i=0}^n f_i \cdot S_i(\phi_i). \quad (1.25)$$

The model parameters  $\phi$  can be fitted to the measured diffusion signals. When the model is chosen carefully, the microstructural properties of the tissue can be inferred directly from the fitted parameters.

#### Bi-exponential model

One of the simplest compartment models is the bi-exponential model, expressing diffusion as the summation of two separate mono-exponential decay curves (see Equation ??) with two different diffusion coefficients (usually named  $\text{ADC}_{slow}$  and  $\text{ADC}_{fast}$ ):

$$S_{biexp}(b) = f_{slow} \exp(-b \cdot \text{ADC}_{slow}) + f_{fast} \exp(-b \cdot \text{ADC}_{fast}). \quad (1.26)$$

Experiments by ? in in-vivo brain data demonstrate good agreement between measurements and fitted signal curves over a range of  $b$ -values. However, the biophysical interpretation of the two compartments is still in debate and the relation between the compartments and the microstructural properties of white matter remains unclear.

### Multi compartment models of nervous tissue

**Stanisz' model** ? were the first to propose a model that reflects the underlying micro-anatomy of nervous tissue. They introduced a model of restricted diffusion in bovine optic nerve using a three-compartment model. In their model, prolate ellipsoids represented axons, glial cells are represented by spheres represented and Gaussian diffusion was assumed in a homogeneous extra-cellular medium surrounded by partially permeable membranes. Experimental data was in agreement with the signal predicted by their model and showed significant departure of the Diffusion Weighted Imaging (DWI) signal from the simple Gaussian model. However, the complexity of this models requires very high quality measurements, typically only achievable in NMR spectroscopy rather than MRI.

**The CHARMED model** Recently, ? developed the CHARMED model of cylindrical axons with gamma distributed radii to estimate axon diameter distributions in white matter tissue. The CHARMED model assumes two compartments, representing diffusion in intra-axonal and extra-axonal space. The intra-axonal compartment is modeled by parallel cylinders, with the size of radii following a gamma-distribution. The extra-cellular compartment is modeled by a DT with the principal diffusion direction  $\vec{v}_1$  aligned with the long cylinder axis. ? validated the model in in-vitro optic and sciatic nerve samples and estimated parameters show good correlation with corresponding histology. In later work, ? extended the CHARMED model by an isotropic diffusion compartment to account for partial volume effects and contributions from areas of CSF. They apply their model to image axon size distributions in the corpus callosum of live rat brain. However, in both experiments, scan times are long and the high 7T magnetic field and maximum  $|G|$  (400 mT/m) are impossible to achieve on a live human scanners, typically operating at 1.5-3T with maximum  $|G|$  between 30-60 mT/m.

**Alexander's minimal model of white matter diffusion** Alexander et al. (2010) uses a simplified CHARMED model to demonstrate measurements of axon diameter and density in excised monkey brain and live human brain on a standard clinical scanner with multi shell high angular resolution diffusion imaging (HARDI). The minimal model of white matter diffusion (MMWDM) expresses diffusion in a white matter voxel as a combination of water particles trapped inside three different compartments:

1. Intra-axonal water experiencing diffusion restricted inside cylindrical axons with equal radius  $R$  as developed by ?
2. Extra-axonal water that is hindered due to the presence of adjacent axons. Diffusion is approximated by a diffusion tensor, with parallel diffusion

coefficient  $d_{\parallel}$  in the direction of the cylinders and symmetric diffusion  $d_{\perp}$  in the perpendicular directions.

3. Water that experiences unhindered diffusion, e.g., in the CSF, modeled by an isotropic Gaussian distribution of displacements with diffusion coefficient  $d_I$ .
4. Non-diffusing water, e.g., trapped in membranes (no parameters).

To reduce the number of free parameters in the model,  $d_{\perp}$  can be expressed by using the tortuosity formulation of ?.

## Active Imaging

More complex models usually require DWI acquisitions with several different diffusion weightings at various diffusion times. For example ? perform approx. 900 different combinations of  $0 \leq |G| \leq 0.3mT$ ,  $0 \leq \delta \leq 0.03ms$  and  $0 \leq \Delta \leq 0.30ms$  to estimate the axon diameter distribution of live rat brain. This extensive sampling of the PGSE parameter space requires long acquisition times (between hours and days) and is infeasible for in-vivo clinical scanning.

The principle of the “Active Imaging” protocol optimisation framework of ? is to find the protocol  $\mathcal{P}$ , that allows the most accurate estimation of the tissue model parameters under given hardware and time constraints. The Fisher information matrix (FIM) provides a lower bound on the inverse covariance matrix of parameter estimates, i.e., the  $\mathcal{P}$  that maximizes the FIM will maximize the precision of those estimates. He uses the d-optimality criterion (?), which is defined as the determinant of the inverse FIM of protocol  $\mathcal{P}$  and tissue model parameters  $\phi$ :

$$D(\phi, \mathcal{P}) = \det[(\mathbf{J}^T \Omega \mathbf{J})^{-1}], \quad (1.27)$$

where  $\mathbf{J}$  is the  $N \times \text{size}(\phi)$  Jacobian matrix with the  $ij$ st element  $\partial S(\vec{g}_i, \delta_i, \Delta_i) / \partial \phi_j$ . In the original approach  $\Omega = \text{diag}\{1, \dots, 1\}$ . ? uses a stochastic optimization algorithm (?) that returns  $\mathcal{P}'$  with minimal  $D$  among all possible  $\mathcal{P}$  with respect to the given scanner hardware limits.

The optimisation framework was used in Alexander et al. (2010) to estimate the parameters of the MMWDM, described in section 1.4.8 using a standard clinical Philips 3T scanner with maximum  $|G|$  of  $60mT/m$  and a maximum scan time of one hour (total number of acquisitions  $N = 360$ ). To achieve estimates independent of fibre orientation, the  $N$  acquisition are divided in  $M$  sets of different PGSE settings with gradient directions in each set being fixed and uniformly distributed over the sphere as in ?. They performed in-vivo scans of the corpus callosum and compared their axon diameter and density indices with high resolution scans of ex-vivo monkey brain and previously published histology studies. They found that the trends in diameter and density agreed with both ex-vivo scans and histology, although the axon diameter was overestimated. This is mainly an effect of limited gradient strength as has been shown in ?.

## Application in the cord

of different PGSE settings and gradient direction one can infer about the directionality of molecule movement with in the tissue.

## 1.5 Summary

We have discussed ways of inferring microstructural information from DWI , ranging from simple methods such as ADC or Diffusion Tensor Imaging (DTI) to sophisticated multi-compartment modelling. ADC and DTI are easy to obtain but the simplistic underlying assumptions of Gaussian displacement probability density function (DPDF) is often inaccurate. As a result, different microstructural changed pathologies can have the same effect on those metrics and therefore cannot be told apart by DTI alone. At least in theory, QSI has the potential to overcome this limitation but requires both very strong diffusion gradients and long acquisition times. Furthermore, QSI derived parameters DPDF measures only relates indirectly to white matter structure and must be carefully interpreted if the SGP is violated.

Using more advanced diffusion models, incorporating anatomical a-priori information about the different compartments of the investigated tissue can overcome the limitations of the simplistic DTI model but at the same time allows more flexibility than QSI. However, in-vivo scans are limited in maximum scan time and hardware capabilities. Under these conditions, finding the optimal set of acquisition parameters is not trivial. The optimisation framework of Alexander can be used to find the DWI protocol that is best suited to estimate the model parameters of interest while it respects the limitations of the clinical setup.

# Bibliography

- Alexander, D. C., Hubbard, P. L., Hall, M. G., Moore, E. A., Ptito, M., Parker, G. J. M., & Dyrby, T. B. (2010). Orientationally invariant indices of axon diameter and density from diffusion MRI. *NeuroImage*.
- R Core Team (2012). *R: A Language and Environment for Statistical Computing*. R Foundation for Statistical Computing, Vienna, Austria. ISBN 3-900051-07-0.  
URL <http://www.R-project.org/>
- Wang, J., Zamar, R., Marazzi, A., Yohai, V., Salibian-Barrera, M., Maronna, R., Zivot, E., Rocke, D., Martin, D., Maechler, M., & Konis., K. (2012). *robust: Insightful Robust Library*. R package version 0.3-19.  
URL <http://CRAN.R-project.org/package=robust>
- Wolak, M. E., Fairbairn, D. J., & Paulsen, Y. R. (2011). Guidelines for estimating repeatability. *Methods in Ecology and Evolution*.